processes

MDPI

Article

Synthesis and Research of Rare Earth Nanocrystal Luminescent Properties for Security Labels Using the Electrohydrodynamic Printing Technique

Chinh Dung Trinh [1,2,3,*,†], Thuan Van Doan [4,†], Phuong Hau Thi Pham [1,2], Dung My Thi Dang [1,2], Pham Van Quan [5] and Chien Mau Dang [1,2,*]

1 Institute for Nanotechnology, Ho Chi Minh City 700000, Vietnam; pthphuong@vnuhcm.edu.vn (P.H.T.P.); dtmdung@vnuhcm.edu.vn (D.M.T.D.)
2 Vietnam National University, Ho Chi Minh City 700000, Vietnam
3 The University of Science, Vietnam National University, Ho Chi Minh City 700000, Vietnam
4 NTT Institute of High Technology, Nguyen Tat Thanh University, Ho Chi Minh City 700000, Vietnam; doanthuanms@gmail.com
5 Hue Industry College 70 Nguyen Hue, Hue City 530000, Vietnam; quanrua@gmail.com
* Correspondence: tdchinh@vnuhcm.edu.vn (C.D.T.); dmchien@vnuhcm.edu.vn (C.M.D.)
† These authors contributed equally.

Received: 1 October 2019; Accepted: 6 January 2020; Published: 24 February 2020

Abstract: YVO_4:Eu^{3+} nanoparticles were successfully synthesized by two methods, namely the sonochemical method and hydrothermal method. The X-ray diffraction (XRD) patterns showed the tetragonal phase of YVO_4 (JCPDS 17-0341) was indexed in the diffraction peaks of all samples. The samples synthesized by the sonochemical method had a highly crystalline structure (X-ray diffraction results) and luminescence intensity (photoluminescence results) than those synthesized by the hydrothermal method. According to the results of field emission scanning electron microscopy (FE-SEM) and transmission electron microscopy (TEM), the average size of YVO_4:Eu^{3+} nanoparticles was around 25–30 nm for the sonochemical method and 15–20 nm for the hydrothermal method. YVO_4:Eu^{3+} nanoparticles in the case of the sonochemical method had a better crystalline structure and stronger emissivity at 618 nm. The Eu^{3+} ions' average lifetime in YVO_4:Eu^{3+} at 618 nm emission under 275 nm excitation were at 0.955 ms for the sonochemical method and 0.723 ms for the hydrothermal method. The security ink for inkjet devices contained YVO_4:Eu^{3+} nanoparticles, the binding agent as polyethylene oxide or ethyl cellulose and other necessary solvents. The device used for security label printing was an inkjet printer with an electrohydrodynamic printing technique (EHD). In the 3D optical profilometer results, the width of the printed line was ~97–167 µm and the thickness at ~9.1–9.6 µm. The printed security label obtained a well-marked shape, with a size at 1.98 × 1.98 mm.

Keywords: luminescent material; nanoparticles; YVO_4:Eu^{3+}

1. Introduction

Recently, researchers have paid attention to an inkjet technique in order to produce spare parts, such as electric circuits and bio-sensors [1–4]. This technique possesses the advantages of reducing steps in preparation and the printing ability in many different substrates, such as conductive, non-conductive, solid or flexible substrates. Besides research on the printing procedure, the most important issue is the preparation of an appropriate ink for a particular application. For that reason, security ink made of rare earth nanoparticles is a current focus as it has a wide application. In 2012, Meruga et al. [5] researched security ink from rare earth nanoparticles using β-$NaYF_4$-doped Yb^{3+}/Er^{3+} and Yb^{3+}/Tm^{3+} in order to print a security QR code on a paper substrate and PET by Optomec direct-write aerosol jetting. In this

research, the thickness of the QR sample printed on the paper substrate was in micrometer and the width in centimeter. A publication by Gupta et al. in 2010 also researched security ink from a rare earth nanoparticle, this time Y_2O_3-doped Eu^{3+} (Y_2O_3:Eu^{3+}), but the printing method was by screen printing devices with a large-size security label, not by inkjet devices [6]. Our research goal is to study the security inkjet technique to enhance its security ability. The utilization of inkjet technology and security ink are emerging in high-security labels for printing money, visas, certificates and military products. There were two keys for the high security requirement: a small delicacy size (related to the printing technique) and strong luminescent intensity of the printed label under UV irradiation (related to optical emissivity of YVO_4:Eu^{3+} nanoparticles in the ink). The luminescent intensity of YVO_4:Eu^{3+} nanoparticles was attributed by many parameters, such as particles size and crystallinity, doped yield of Eu^{3+} ions into YVO_4, etc. A producible method need optimum synergy of these parameters [7–9].

In this report, two methods, namely the sonochemical and hydrothermal methods, were experimented with for the YVO_4:Eu^{3+} synthesis. According to a published work, a doped ratio at 5 mol % is the most appropriate ratio for luminescent intensity [9–14], which was also our doped ratio of the Eu^{3+} ion. YVO_4:Eu^{3+} nanoparticles in the sonochemical method resulted the strongest luminescent intensity, which was used as red phosphor secured ink. Two types of security ink were prepared with different binding agents and solvent ingredients, and lead to different surface tensions. Using the electrohydrodynamic printing technique (EHD) inkjet printer, the line of the security label had width at ~97–167 μm and thickness at ~3–5 μm. The security labels were printed with various nanoparticle sizes, but the specific size was at 1.98 × 1.98 mm and the minimum distance between the two droplets was controlled at 0.05 μm.

2. Experimental

2.1. Material

Y $(NO_3)_3.6H_2O$ (99.8%, Aldrich, St. Louis, MO, USA), Eu $(NO_3)_3{\cdot}5H_2O$ (99.9%, Aldrich, St. Louis, MO, USA) and Na_3VO_4 (99.98%, Aldrich, St. Louis, MO, USA) were used right after being unpacked as initial materials. NaOH (99%, Merck, Darmstadt, Germany) was used to control pH.

Poly (ethylene oxide)-PEO 100.000 (Aldrich, St. Louis, MO, USA), chloroform (99.5%, Aldrich, St. Louis, MO, USA), ethyl cellulose (Aldrich, St. Louis, MO, USA), α-terpinoel (99%, Aldrich, St. Louis, MO, USA), isopropanol (99.5%, Aldrich, St. Louis, MO, USA) and deionized water were binding agents and solvents used in the synthesis of the security ink.

2.2. Synthesis of YVO_4:Eu^{3+} Nanoparticles

YVO_4:Eu^{3+} nanoparticles were synthesized by the wet chemical method. Solution A was prepared by dissolving 0.88 g of $Y(NO_3)_3{\cdot}6H_2O$ (2.3 mmol) and 0.05g of $Eu(NO_3)_3{\cdot}5H_2O$ (0.12 mmol) into 15 mL deionized water (Eu^{3+} doping molar concentration was 5%) for 15 min under stirring. Solution B was formed by dissolving 0.44 g of Na_3VO_4 (2.4 mmol) in 15 mL deionized water. Next, solution A and solution B were dropwise mixed until a white precipitation formed in the solution. The pH value of the solution was adjusted to 12 by adding 5M of NaOH. The mixture was then heated by two methods:

- The sonochemical method: The mixture was ultrasonicated in 10 min, at a frequency of 20 kHz (Ultrasonic Liquid Processors VCX 750) made by Sonics & Materials (Newtown, CT, USA).
- The hydrothermal method: The mixture was poured in Teflon sealed tightly and placed in the autoclave oven at 200 °C for one hour.

2.3. Preparation of Security Inkjet Ink

Two kinds of security inkjet inks using YVO_4:Eu^{3+} nanoparticles were prepared by mixing YVO_4:Eu^{3+} nanoparticles with a binding agent and solvents in the appropriate ratio (Table 1).

Table 1. The ingredient components of the printing inks.

	$YVO_4:Eu^{3+}$ Powder (wt %)	Polyethylene Oxide (wt %)	Chloroform (wt %)	Deionized Water (wt %)	Ethyl Cellulose (wt %)	α-Terpinoel (wt %)	Isopropanol (wt %)
Ink I	8	49	23	20	0	0	0
Ink II	8	0	0	0	6	92	4

2.4. Security Printing

The test patterns were printed on a glass substrate by a commercial printer (PS JET 300V, Printing Solution, Seoul, Korea) using the electrohydrodynamic (EHD) inkjet technique.

2.5. Characterization

The synthesized $YVO_4:Eu^{3+}$ nanoparticles samples were studied by field emission scanning electron microscopy (SU8010, Hitachi, Tokyo, Japan) and transmission electron microscopy (TEM, JEOL, Tokyo, Japan). The crystalline structure and doping of $YVO_4:Eu^{3+}$ has been analyzed by X-ray diffraction spectroscopy and Raman spectroscopy. The excitation and emission spectra were recorded at room temperature through a Hitachi F-4500 spectrofluorometer (Hitachi, Tokyo, Japan). The luminescence time decay was measured by a DeltaflexTM (Horiba, Kyoto, Japan) with a 275 nm SpectraLED excitation source.

The surface tension of the security ink was analyzed by optical contact angle and the surface tension meter KSV CAM 101 (KSV Instruments, Monroe, CT, USA). The viscosity of the security ink was analyzed by a m-VROC™ VISCOMETER (RheoSense, San Ramon, CA, USA). The printed samples were analyzed by a 3D optical profilometer (Sensofar Metrology, Barcelona, Spain) and UV 20 W mercury lamps of 254 nm (Germicidal lamp, Sankyo Denki Co., Kanagawa, Japan). The ink droplet which jetted out of the printer was imaged by high-speed camera (FASTCAM SA-Z, Photron, Tokyo, Japan).

3. Results and Discussion

The purpose of this study is to provide a synthesis of strong luminescent intensity $YVO_4:Eu^{3+}$ nanoparticles for application in security ink as a luminescent substance. Many factors may affect the light emission of $YVO_4:Eu^{3+}$ nanoparticles (related to the light-emitting mechanism), such as the doping ratio of Eu^{3+} ions, the particle crystalline growth and the nanoparticle size. With the same chemical components and ratio (the doping concentration of Eu^{3+} was 5 mol %), the different correspondences of $YVO_4:Eu^{3+}$ nanoparticles that were found were due to the two synthesis methods, sonochemical or hydrothermal.

According to Figure 1a–c, there is an appearance of sphere morphology in $YVO_4:Eu^{3+}$ nanoparticles from the hydrothermal method, whereas no sphere was found in the sonochemical method. The $YVO_4:Eu^{3+}$ nanoparticle size of both the sonochemical and hydrothermal methods is mainly at 25–30 nm and 15–20 nm, respectively. The $YVO_4:Eu^{3+}$ nanoparticles size synthesized by two methods is suitable for the preparation of security ink. Figure 1d shows the XRD patterns of the $YVO_4:Eu^{3+}$ nanoparticle crystalline prepared by the two different methods. YVO_4 tetragonal phase (JCPDS, No. 17-0341) represented by all the diffraction peaks confirmed the existence of a crystalline structure in all nanoparticles [15–20]. The presence of additional peaks indicated that the Eu^{3+} ions have been successfully built into the YVO_4 host lattice. However, the peaks in the sonochemical method have a clear appearance with higher $YVO_4:Eu^{3+}$ nanoparticle crystallinity than when using the hydrothermal method.

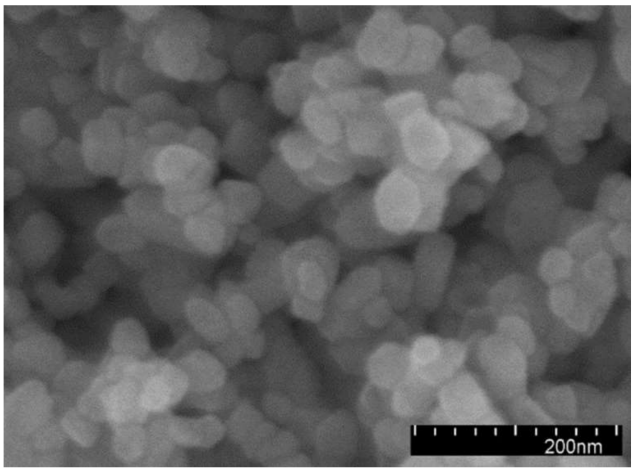

(**a**)

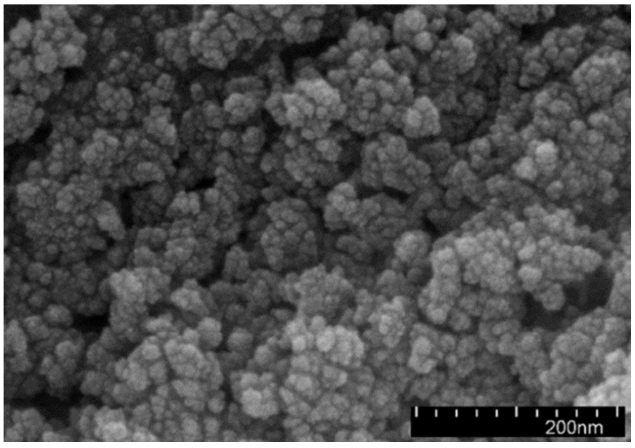

(**b**)

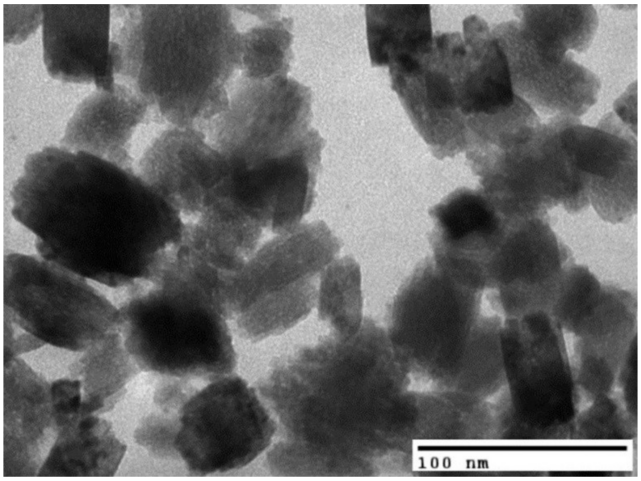

(**c**)

Figure 1. *Cont*.

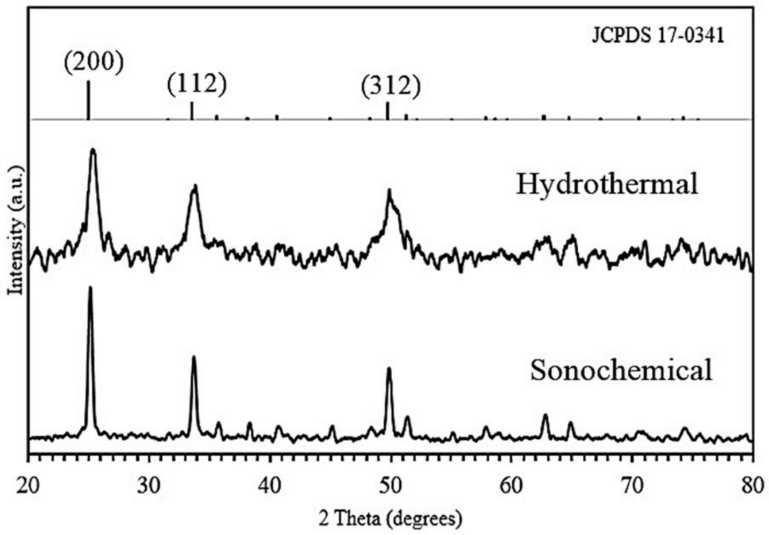

(**d**)

Figure 1. FE-SEM micrographs of YVO_4:Eu^{3+} nanoparticles synthesized by the sonochemical (**a**) and hydrothermal (**b**) methods. TEM micrographs of YVO_4:Eu^{3+} nanoparticles synthesized by the sonochemical method (**c**). XRD patterns of YVO_4:Eu^{3+} nanoparticles synthesized by different methods (**d**).

Figure 2 shows the energy dispersive X-ray (EDX) spectra of YVO_4:Eu^{3+} nanoparticles synthesized by the sonochemical and hydrothermal methods. According to the EDX spectrum in the two samples of YVO_4:Eu^{3+} nanoparticles, there exists yttrium (Y), oxygen (O), vanadium (V) and europium (Eu) elements, indicating that Eu^{3+} ions were doped into the YVO_4 nano-crystals.

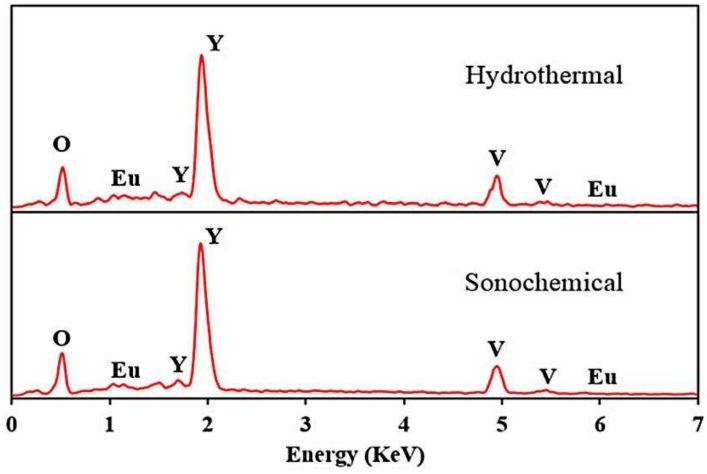

Figure 2. EDX spectra of YVO_4:Eu^{3+} nanoparticles synthesized by sonochemical and hydrothermal methods.

Figure 3a shows the Raman spectra of undoped and Eu-doped YVO_4 nanoparticles synthesized at different methods. The undoped YVO_4 sample is synthesized by the hydrothermal method with the same chemical ratio as two doped samples. The YVO_4 crystal in the tetragonal structure is attributed to the point group of D_{4h}. The vibration appearance of complex VO_4^{3-} and Y^{3+} ions in YVO_4 unit cells produce the lowest vibrational frequency at 164 cm^{-1} as external modes of Raman spectra [15]. The six Raman modes of these crystals were at 260, 379, 488, 813, 839 and 893 cm^{-1} (internal modes) [15,16]. There is a red shift of 388 cm^{-1} belonging to the undoped YVO_4 to the weaker

wavelength at 379 cm^{-1} (Figure 3b). Furthermore, the intensity ratio difference between the two typical modes is at 839 and 893 cm^{-1} (Figure 3c), presenting a significant change between doped and undoped samples. The doping frequently causes the expansion or contraction of the crystal lattice depending on the difference between the ionic radius of the dopant and host cations. The replacement of Y^{3+} ions by relatively larger Eu^{3+} ions causes a stretching of the host lattice which can decrease the phonon energies causing a shift of the Raman modes [7,11,13,17]. The result of Raman spectra shows that the lattice vibration of the YVO_4 structure is altered due to the occupancy of the Eu ions at Y^{3+} sites in the YVO_4 host lattice.

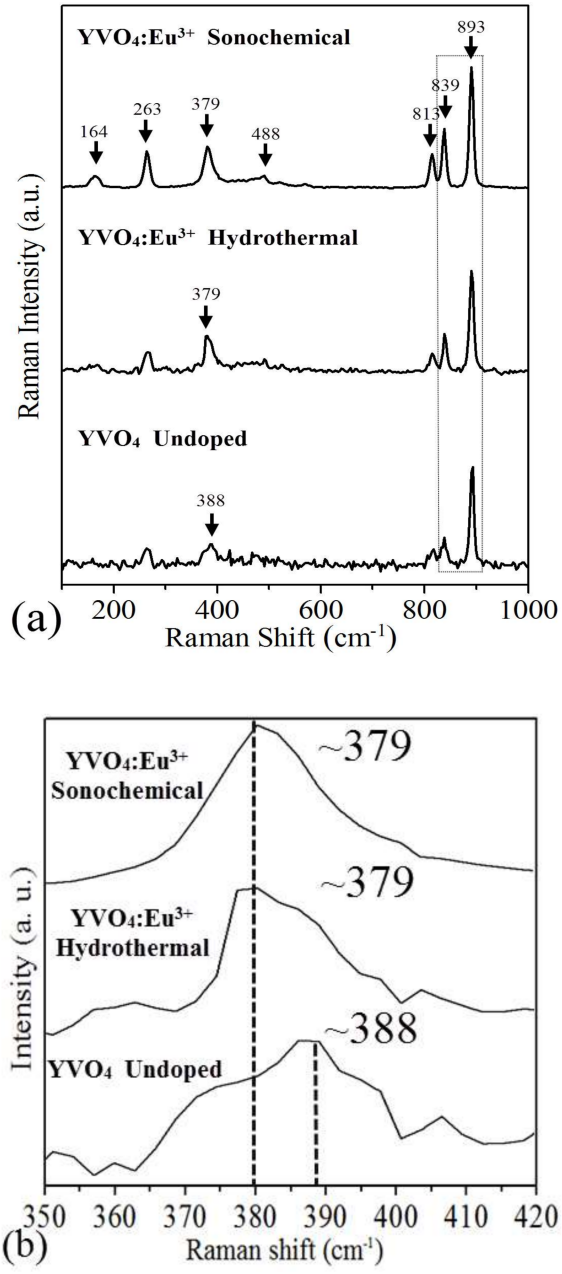

Figure 3. *Cont.*

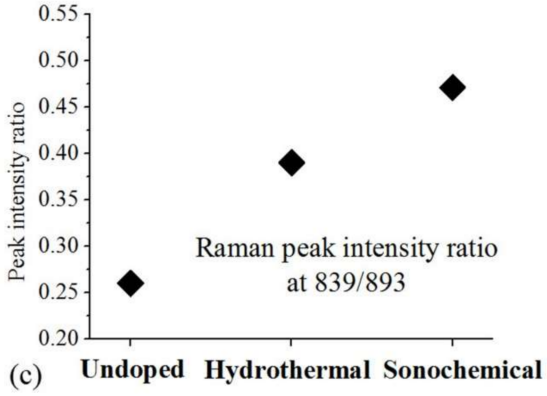

Figure 3. Raman spectra of undoped and Eu-doped YVO_4 nanoparticles synthesized by the sonochemical and hydrothermal methods (**a**). The Raman active mode shift at 388 cm^{-1} for undoped and Eu-doped YVO_4 nanoparticles (**b**). The Raman peak intensity ratio diagram at 839 and 893 cm^{-1} (**c**).

Figure 4a shows the YVO_4:Eu^{3+} luminescence mechanism. There are three major steps in the excitation and emission process of YVO_4:Eu^{3+} under UV radiation. First, the absorption of UV radiation by VO_4^{3-} groups. Second, the migration of thermal activated energy (comes from the UV excitation source) through the vanadate sub-lattice, causing the transferring of excited energy to Eu^{3+} ions. Last, the appearance of strong red emissions due to the de-excitation process of excited Eu^{3+} ions [11,13,18,21–23].

Figure 4b shows the correspondence of the excited photoluminescence (PLE) spectra of the 618 nm emissions to Eu^{3+}: $^5D_0 \rightarrow {}^7F_2$ transition of theYVO_4: Eu^{3+} nanoparticles. There is an intensive broadband consistence, ranging from 260 to 350 nm, which occurred in all excited spectra. The origin of the broadband is supposed by O^{2-}–V^{5+} within the VO_4^{3-} group charge transfer. There is the respective attribution of several weak narrow bands in the range of 350–550 nm to the f–f transitions within the $4f^6$ configuration of the Eu^{3+} ions. The Eu^{3+} f–f transitions have a weak absorption intensity in comparison to that of the VO_4^{3-} groups, indicating that the Eu^{3+} ions excitation is mainly created by the VO_4^{3-} groups, and energy transfer from the VO_4^{3-} groups to Eu^{3+}ions [18–40].

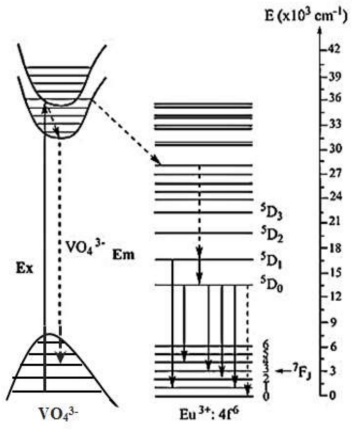

(**a**)

Figure 4. *Cont.*

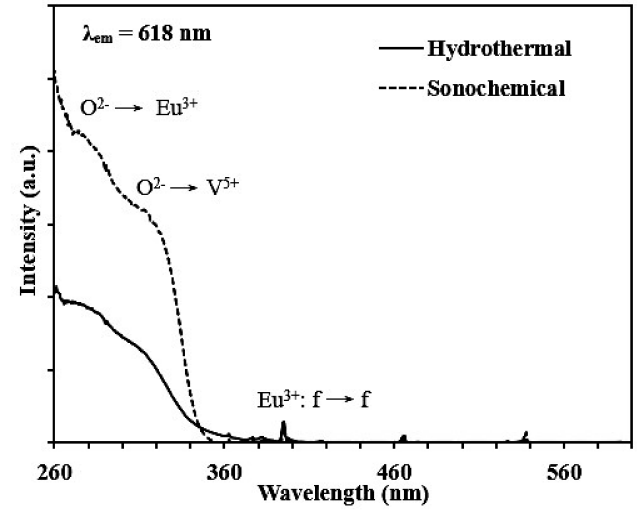

(**b**)

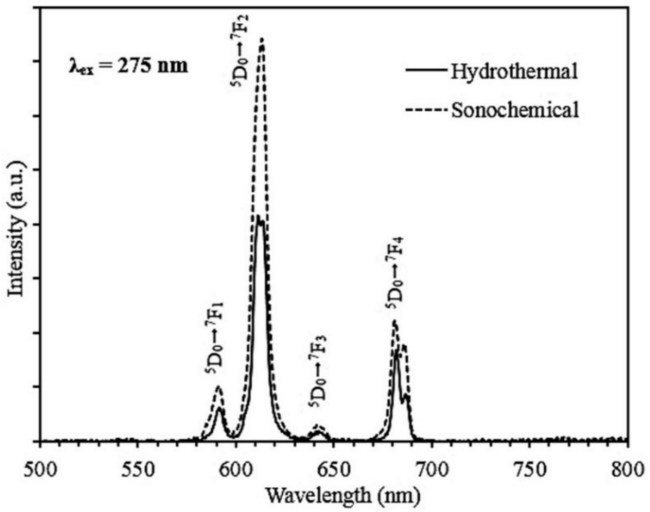

(**c**)

Figure 4. Energy levels and transitions scheme of Eu^{3+}, vertical arrows: absorption and emission transitions (**a**). Photoluminescence excitation (PLE) spectra (**b**) and photoluminescence emission (PL) spectra of samples with different methods (**c**).

In Figure 4c, the specific peaks appear at 590, 618, 645 and 690 nm as a result of the $^5D_0 \rightarrow ^7F_1$ (magnetic-dipole transition), $^5D_0 \rightarrow ^7F_2$ (electric-dipole transition), $^5D_0 \rightarrow ^7F_3$ and $^5D_0 \rightarrow ^7F_4$ (excited optical source at approximately 275 nm) transfer. The main emission is at 618 nm by strongest emissivity $^5D_0 \rightarrow ^7F_2$. In this research, the red emission of YVO_4:Eu^{3+} nanoparticles was analyzed (peak at 618 nm). At 618 nm, the luminescent intensity of the sample synthesized by the sonochemical method is stronger than the one using the hydrothermal method. This is again confirmed with the XRD patterns above. In the sonochemical method, particles have a better crystallinity due to a high local temperature and pressure during the growing. The result in Figure 4c also indicates the occupying of Eu^{3+} ions in the asymmetry inversion center instead of Y^{3+} in both methods.

In Figure 5, the room-temperature luminescence decay curves of the $^5D_0 \rightarrow ^7F_2$ transition of Eu^{3+} are presented for the samples synthesized in both methods. The excitation wavelength is fixed at 275 nm. The common factors that affect to the decay kinetics behavior are the number of different

luminescent centers, defects, energy transfer and host impurities [41]. The raw recorded data for the decay curves of all samples are well-fitted by a double-exponential function, descripted as below:

$$I = A_1\exp(-t/\tau_1) + A_2\exp(-t/\tau_2)$$

where I is the luminescence intensity at time t. A_1, A_2 are the fitting parameter and τ is the decay lifetime, respectively. The Eu^{3+} ions' average lifetime in the samples synthesized by sonochemical and hydrothermal methods at 618 nm emission under 275 nm excitation are 0.955 and 0.723 ms. The average lifetime increases for the sonochemical method sample. The non-radiative transition by the surface defects and/or crystallinity rate causes the appearance of a decay lifetime difference [8]. The surface effect has a great impact on the properties of the material at the nanometer size. In the nanocrystal, the defects of the lattice commonly appear on the surface. The surface defects cause the decreasing of lifetime and luminescent intensity. With sonochemical method, YVO_4:Eu^{3+} nanoparticles have better crystallization due to a high local temperature and pressure, and the lower surface effect. Furthermore, decay time is measured in both radiative and nonradiative transmission. The radiative decay component is depended on the number of light-emitting activator ions in the nanoparticles [19]. The Eu^{3+}-doped ions in the host lattice are light emitting activators, showing the better Eu^{3+} ion occupancy to Y^{3+} sites in the sample when synthesized by the sonochemical method compared to the hydrothermal method.

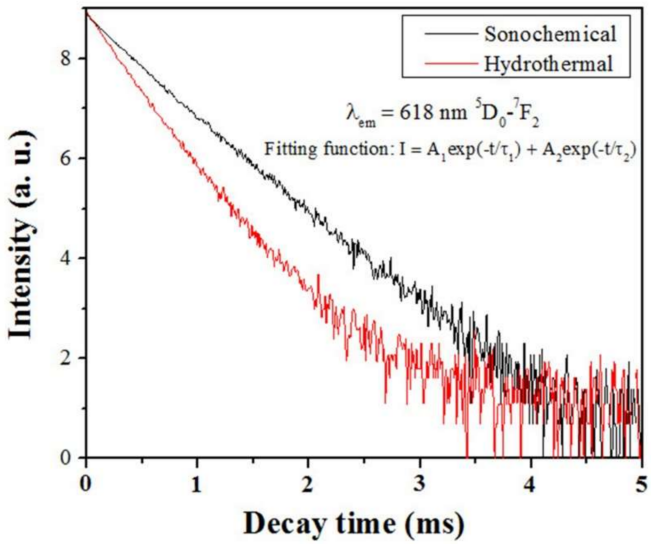

Figure 5. The luminescence decay curves for the $^5D_0$ excited state of Eu^{3+} under 275 nm excitation for YVO_4:Eu^{3+} samples synthesized with different methods.

Due to the stronger luminescent intensity and more compatible nanoparticle size, YVO_4:Eu^{3+} nanoparticles synthesized by the sonochemical method are primarily used in the preparation of security ink. Two type of printing ink are prepared with same mass ratio of YVO_4:Eu^{3+} nanoparticles powder but different solvent ingredients. The ingredients of printing ink are shown in Table 1.

The viscosity and surface tension of printing ink are very important in the preparation of patterns using the inkjet technique due to the huge influence in spraying ink out of a head nozzle [42,43]. The analyzed and calculated parameters of ink I and II are presented in Table 2. All these parameters are analyzed under room temperature. Figure 6 presents the diagram of analyzed surface tension of ink I and ink II. Ink I's surface tension is ~46–47 mN/m, whereas ink II's is ~38–40 mN/m. The average viscosity of ink I and ink II, in turn, is ~119 and 108 cP (Table 2). The parameters of the prepared inks are in good working range of the inkjet device. The pattern is printed onto a glass substrate by a commercial printer PS JET 300V operated by the electrohydrodynamic (EHD) inkjet technique.

Table 2. The printing parameters of inks I and II.

	Viscosity (cP)	Surface Tension (mN/m)	Density (g/cm^3)
Ink I	119	46.3	1.15
Ink II	108	38.2	1.32

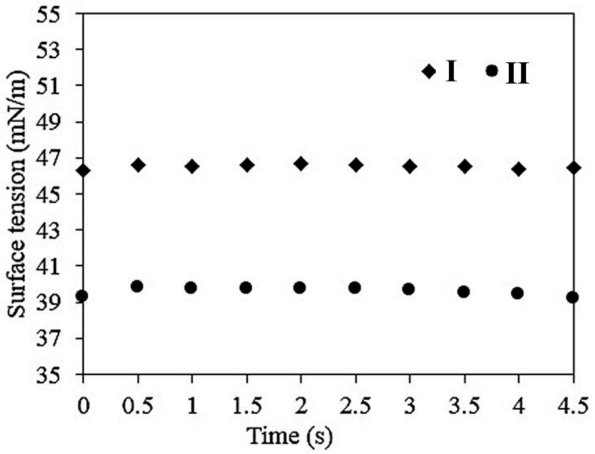

Figure 6. The diagram of analyzed ink surface tension.

Figure 7 shows the mechanism of EHD technology. The application of electrohydrodynamic inkjet technique with positive pressure and high-voltage in the nozzle is to spray a fine droplet or thin line [44,45]. The EHD technique usage in pattern preparation required the adjustment of many parameters in the printing devices. This is an important step which the direction of the inkjet are performed. The parameter for the printing device has been adjusted after many experiments and established the standard parameter, showed in Table 3.

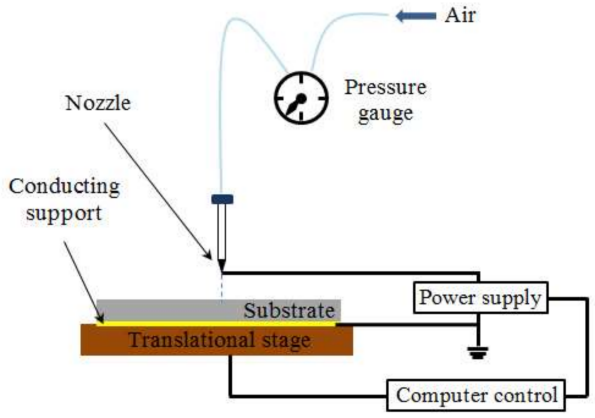

Figure 7. Schematic of the electrohydrodynamic (EHD) technology mechanism.

Table 3. The parameter conditions of printing.

Pressure (kPa)	DC Volt (V)	AC Volt (V)	Frequency (Hz)	Distance between Printhead and Substrate (μm)
11–15	500–550	700–900	500	100–150

These parameters are used to print both ink I and ink II. The diameter of the printhead nozzle is one of the most important factors influencing the size of ink droplet when contacting to substrate (related to printed patterns size and sharpness). The smaller the printhead nozzle, the smaller the droplet size.

Figure 8 shows the picture of an ink droplet jetted onto a glass substrate, using ink II (Figure 8a) and ink I (Figure 8b). The process of an ink droplet jetted onto the glass substrate is shown in three continuous pictures taken by high speed camera with frame rate set at 1000 frames per second. According to the frame rate, the time for an ink droplet to be jetted onto the substrate (from start to finish) is around 0.002 s. With a diameter of the print head at ~15 µm, the droplet size on the substrate is at ~10 µm with ink II and ~2 µm with ink I. The surface tension difference between ink I and ink II causes this phenomenon (with the same viscosity, the surface tension of ink I being higher than ink II). Due to the characteristic differences, each security ink can be applied for separate security label printings.

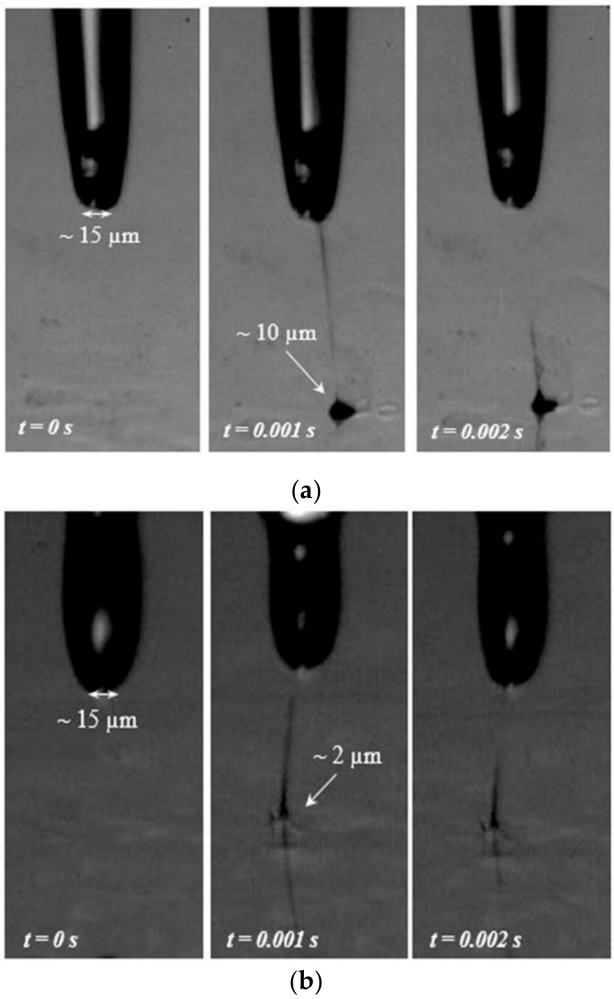

Figure 8. Image taken by high speed camera of an ink droplet jetted onto a glass substrate, performing of ink II (**a**) and ink I (**b**).

The purpose of this process is to adjust the printing parameters by observing the ink jetting out of the printhead. In Figure 9a,b, the width of lines printed by ink I was ~97–115 µm and by ink II ~135–167 µm. All lines are sharp and seamless. Figure 9c,d show a clear appearance of security labels with an actual diameter at 1.98 mm × 1.98 mm (printed by ink I). The printed security label size may vary depending on the label shape. With this result, there is a possibility to print labels of a few hundred micrometers in size (by both ink I and ink II). Downsizing the label may increase the security

ability. The continuous improving of the ink and the printing process is contributed to the printing ability on different types of substrate with higher sharpness and a few micrometers size.

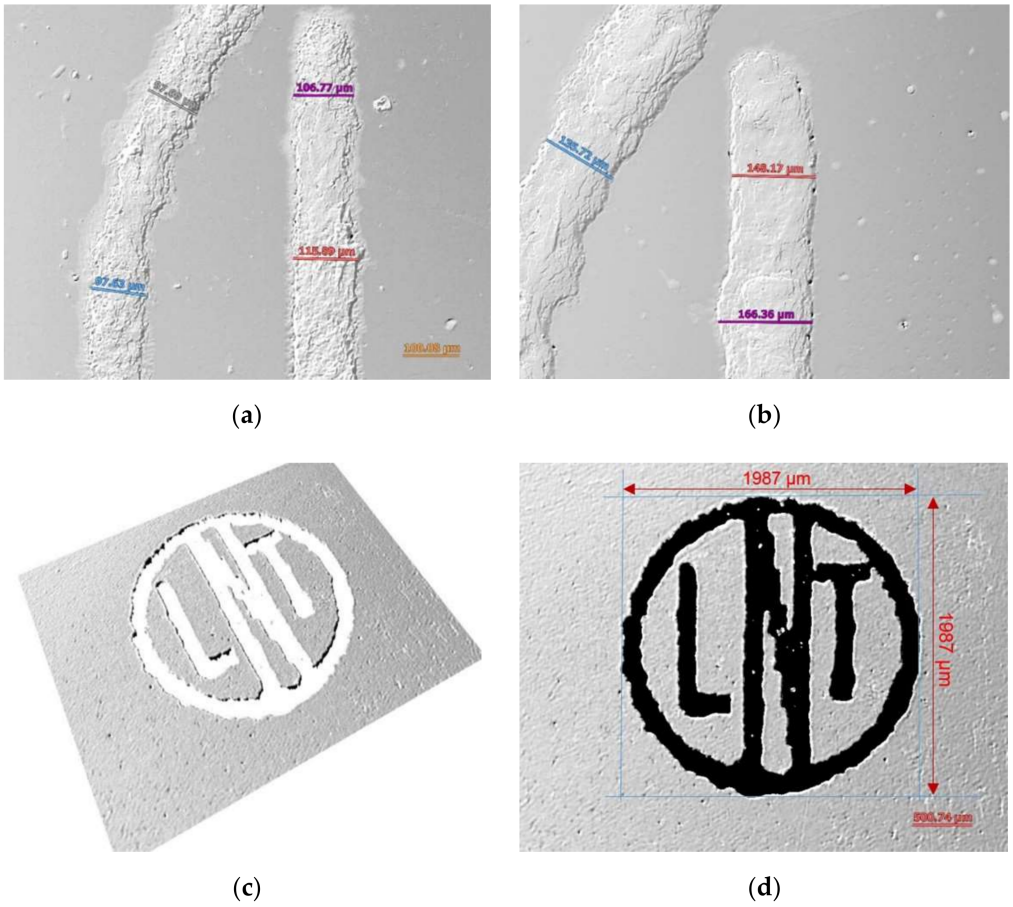

(**a**) (**b**)

(**c**) (**d**)

Figure 9. The micrographs from a 3D optical profilometer of a security label's lines printed by ink I (**a**) and ink II (**b**). The micrograph of the security label printed by ink I (**c**,**d**)

Figure 10 shows the height–width diagram of lines printed by ink I and II. The size of the lines printed by ink I is smaller than those printed by ink II, conforming with the results shown in Figure 8. The thicknesses of the labels are, respectively, ~10.8 and 13.5 µm and the widths are ~110 µm and 145 µm. Figure 10b presents the image of a label printed in different sizes on a glass substrate under daylight and UV lamp. The labels are nearly transparent under daylight and have a red color luminescence under a UV lamp with a wavelength of 254 nm. The line appearance is clear, sharp, seamless and does not overlap one another at small distances.

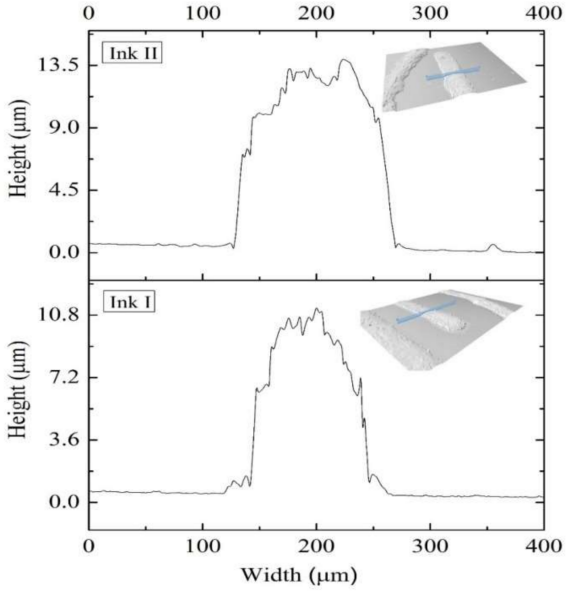

(**a**)

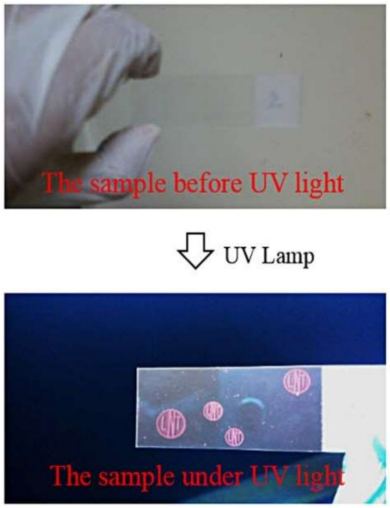

(**b**)

Figure 10. The height–width diagram of the printed lines by ink I and II taken by a Sensofar Metrology 3D Optical Profilometer (**a**). The image of a label under daylight and UV lamp (**b**).

4. Conclusions

YVO_4:Eu^{3+} nanoparticles were synthesized by sonochemical and hydrothermal methods. According to the analysis results, YVO_4:Eu^{3+} nanoparticles were crystallized in the tetragonal structure and exhibited the strongest luminescence at a wavelength of 618 nm due to the $^5D_0 \rightarrow {}^7F_2$ transition. The Eu^{3+} ions' average lifetime in the samples synthesized by sonochemical and hydrothermal methods at 618 nm emission under 275 nm excitation were 0.955 and 0.723 ms. The sonochemical method created the high local temperature, which had a positive effect on the YVO_4:Eu^{3+} nanoparticles crystalline formation and Eu^{3+} ions into the Y^{3+} doping position. Thus, YVO_4:Eu^{3+} nanoparticles synthesized by the sonochemical method possessed a higher crystallinity and better luminescence intensity. The TEM and FE-SEM results showed the average size of the YVO_4:Eu^{3+} nanoparticles was about 23–30 nm under the sonochemical method and about 15–20 nm under the hydrothermal method.

YVO_4:Eu^{3+} nanoparticles synthesized by the sonochemical method had a higher luminescent intensity and compatible particle size, which might be used as red phosphor in security ink. The security labels were printed by inkjet printers using the electrohydrodynamic printing technique. The widths of the printed line were ~97–167 μm and ~3–5 μm were the thicknesses. The properties of the printed security labels (the size at 1.98 mm × 1.98 mm) were a well-sharp shape, daylight invisibility and red emission under UV mercury lamps (wavelength ~254 nm). The high-security labels require a small size, shape sharpness and high luminescence. The minimum controllable diameter of an ink droplet on a glass substrate was ~2 μm, a good base for printed security labels with high sharpness and micrometer size in the future.

Author Contributions: C.D.T. and D.M.T.D. designed the experiments with technical contributions from C.M.D.; C.D.T., T.V.D. and P.H.T.P. performed the experiments and analyzed the data; C.D.T., P.V.Q. and C.M.D. wrote the paper. All authors have read and agreed to the published version of the manuscript.

Funding: This research was funded by Ministry of Science and Technology of Vietnam under the grant number 03/2019/HĐ-SPĐP.

Acknowledgments: The authors highly appreciate the financial support of Ministry of Science and Technology of Vietnam under the grant number 03/2019/HĐ-SPĐP.

Conflicts of Interest: The authors declare no conflict of interest.

References

1. Bidoki, M.S.; Lewis, M.D.; Clark, M. Ink-jet fabrication of electronic components. *J. Micromech. Microeng.* **2007**, *17*, 967–974. [CrossRef]
2. Park, K.B.; Kim, D.; Jeong, S. Direct writing of copper conductive patterns by ink-jet printing. *Thin Solid Film.* **2007**, *515*, 7706–7711. [CrossRef]
3. Apilux, A.; Ukita, Y.; Chikae, M.; Chailapakul, O.; Takamura, Y. Development of automated paper-based devices for sequential multistep sandwich enzyme-linked immunosorbent assays using inkjet printing. *Lab Chip* **2013**, *13*, 126–135. [CrossRef] [PubMed]
4. Dang, M.C.; Dang, T.M.D.; Fribourg-Blanc, E. Inkjet printing technology and conductive inks synthesis for microfabrication techniques. *Adv. Nat. Sci.* **2013**, *4*, 15009–15016. [CrossRef]
5. Meruga, M.J.; Cross, M.W.; May, S.P.; Luu, A.Q.; Crawford, A.G.; Kellar, J.J. Security printing of covert quick response codes using upconverting nanoparticle inks. *Nanotechnology* **2012**, *23*, 395201–395210. [CrossRef] [PubMed]
6. Gupta, K.B.; Haranath, D.; Saini, S.; Singh, N.V.; Shanker, V. Synthesis and characterization of ultra-fine Y_2O_3:Eu^{3+} nanophosphors for luminescent security ink applications. *Nanotechnology* **2010**, *21*, 055607–055615. [CrossRef]
7. Georgescu, S.; Cotoi, E.; Voiculescu, M.A.; Toma, O. Effects of particle size on the luminescence of YVO_4:Eu nanocrystals. *Rom. Rep. Phys.* **2008**, *60*, 947–955.
8. Shao, B.; Zhao, Q.; Guo, N.; Jia, Y.; Lv, W.; Jiao, M.; Lü, W.; You, H. Monodisperse YVO_4:Eu^{3+} submicrocrystals: Controlled synthesis and luminescence properties. *CrystEngComm* **2013**, *15*, 5776–5783. [CrossRef]
9. Bao, A.; Lai, H.; Yang, Y.; Liu, Z.; Tao, C.; Yang, H. Luminescent properties of YVO_4:Eu/SiO_2 core–shell composite particles. *J. Nanopart. Res.* **2010**, *12*, 635–643. [CrossRef]
10. He, F.; Yang, P.; Niu, N.; Wang, W.; Gai, S.; Wang, D.; Lin, J. Hydrothermal synthesis and luminescent properties of YVO_4: Ln^{3+} (Ln = Eu, Dy, and Sm) microspheres. *J. Colloid Interface Sci.* **2010**, *343*, 71–78. [CrossRef]
11. Riwotzki, K.; Haase, M. Wet-chemical synthesis of doped colloidal nanoparticles: YVO_4:Ln (Ln = Eu, Sm, Dy). *J. Phys. Chem. B* **1998**, *102*, 10129–10135. [CrossRef]
12. Wang, H.H.; Odawara, O.; Wada, H. Facile and chemically pure preparation of YVO_4:Eu^{3+} colloid with novel nanostructure via laser ablation in water. *Sci. Rep.* **2016**, *6*, 20507–20515. [CrossRef] [PubMed]
13. Georgescu, S.; Cotoi, E.; Voiculescu, M.A.; Toma, O.; Matei, C. Reflectance spectra of YVO_4: Eu^{3+} phosphors synthesized by direct precipitation. *Rom. J. Phys.* **2010**, *55*, 750–757.

14. Zhang, Y.; Xu, J.; Cui, Q.; Yang, B. Eu^{3+}-doped $Bi_4Si_3O_{12}$ red phosphor for solid state lighting: Microwave synthesis, characterization, photoluminescence properties and thermal quenching mechanisms. *Sci. Rep.* **2017**, *7*, 42464–42476. [CrossRef]
15. Qiao, Y.B.; Liu, X.F.; Zhang, Q.; Chen, D.P.; Wang, Y.W.; Ma, W.B. Synthesis and luminescence properties of YVO_4:Eu nanocrystals grown in nanoporous glass. *Mater. Lett.* **2010**, *64*, 1306–1308.
16. Zhang, S.; Liang, Y.; Gao, Y.X.; Liu, T.H. Hydrothermal synthesis and microstructural, optical properties characterization of YVO4 phosphor powder. *Acta Phys. Pol. A* **2014**, *125*, 105–110. [CrossRef]
17. Kumar, Y.; Pal, M.; Herrera, M.; Mathew, X. Effect of Eu ion incorporation on the emission behavior of Y_2O_3 nanophosphors: A detailed study of structural and optical properties. *Opt. Mater.* **2016**, *60*, 159–168. [CrossRef]
18. Young, S.C.; Young, D.H. Photoluminescence properties of YVO_4:Eu nanophosphors prepared by the hydrothermal reaction. *Bull. Korean Chem. Soc.* **2010**, *31*, 2368–2370.
19. Kumar, V.; Khan, F.A.; Chawla, S. Intense red-emitting multi-rare-earth doped nanoparticles of YVO_4 for spectrum conversion towards improved energy harvesting by solar cells. *J. Phys. D* **2013**, *46*, 365101–365108. [CrossRef]
20. Young, S.C.; Young, D.H. Preparation of transparent red-emitting YVO_4:Eu nanophosphor suspensions. *Bull. Korean Chem. Soc.* **2011**, *32*, 335–337.
21. Natacha, D.; Chrystel, A.; Franck, P.; David, P.; Bruno, V.; Karine, V.; Denis, A.; Clément, S. New synthesis strategies for luminescent YVO4:Eu and EuVO4 nanoparticles with H2O2 selective sensing properties. *Chem. Mater.* **2015**, *27*, 5198–5205.
22. Li, H.Y.; Zang, F.G.; Ma, J. Synthesis and luminescence properties of YVO_4:Eu^{3+} nanocrystals by a Sol-Gel method. *Adv. Mater. Res.* **2013**, *634*, 2268–2271. [CrossRef]
23. Huignard, A.; Buissette, V.; Laurent, G.; Gacoin, T.; Boilot, P.J. Synthesis and characterizations of YVO4:Eu colloids. *Chem. Mater.* **2002**, *14*, 2264–2269. [CrossRef]
24. Van Uitert, L.G. Characterization of energy transfer interactions between rare earth ions. *J. Electrochem. Soc.* **1967**, *114*, 1048–1053. [CrossRef]
25. Struck, C.W.; Fonger, W.H. Quantum-mechanical treatment of Eu^{3+} 4f→4f and 4f? charge-transfer-state transitions in Y_2O_2S and La_2O_2S. *J. Chem. Phys.* **1976**, *64*, 1784–1790. [CrossRef]
26. Nicholas, V.J. Origin of the luminescence in natural Zircon. *Nature* **1967**, *215*, 1476. [CrossRef]
27. Dong, H.; Kuzmanoski, A.; Wehner, T.; Müller-Buschbaum, K.; Feldmann, C. Microwave-assisted polyol synthesis of water dispersible red-emitting Eu^{3+}-modified carbon dots. *Materials* **2017**, *10*, 25. [CrossRef] [PubMed]
28. Steudel, F.; Johnson, A.J.; Johnson, E.C.; Schweizer, S. Characterization of Luminescent Materials with Eu Mössbauer Spectroscopy. *Materials* **2018**, *11*, 828. [CrossRef]
29. Blasse, G.; Grabmaier, B.C. *Luminescent Materials*; Springer: Berlin/Heidelberg, Germany, 1994.
30. Schweizer, S.; Hobbs, L.W.; Secu, M.; Spaeth, J.M.; Edgar, A.; Williams, G.V.M. Photostimulated luminescence in Eu-doped fluorochlorozirconate glass ceramics. *Appl. Phys. Lett.* **2003**, *83*, 449. [CrossRef]
31. Aitasalo, T.; Deren, P.; Hölsä, J.; Jungner, H.; Krupa, J.C.; Lastusaari, M.; Legendziewicz, J.; Niittykoski, J.; Strek, W. Persistent luminescence phenomena in materials doped with rare earth ions. *J. Solid State Chem.* **2003**, *171*, 114–122. [CrossRef]
32. Ten Kate, O.M.; Vranken, T.; van der Kolk, E.; Jansen, A.P.; Hintzen, H.T. Optical properties of Eu^{2+}/Eu^{3+} mixed valence, silicon nitride based materials. *J. Solid State Chem.* **2014**, *213*, 126–131. [CrossRef]
33. Van Dijk, J.M.F.; Schuurmans, M.F.H. On the nonradiative and radiative decay rates and a modified exponential energy gap law for 4f–4f transitions in rare earth ions. *J. Chem. Phys.* **1983**, *78*, 5317. [CrossRef]
34. Shionoya, S.; Yen, W.M.; Yamamoto, H. (Eds.) *Phosphor Handbook*; CRC Press: Boca Raton, FL, USA, 2006.
35. Samanta, T.; Hazra, C.; Mahalingam, V. C-dot sensitized Eu^{3+} luminescence from Eu^{3+}-doped LaF_3-C dot nanocomposites. *New J. Chem.* **2016**, *39*, 106–109. [CrossRef]
36. Kumar, A.; Rai, D.K.; Rai, S.B. Optical studies of Eu^{3+} ions doped in tellurite glass. *Spectrochim. Acta Part A* **2002**, *58*, 2115–2125. [CrossRef]
37. Kemere, M.; Sperga, J.; Rogulis, U.; Krieke, G.; Grube, J. Luminescence properties of Eu, RE^{3+} (RE = Dy, Sm, Tb) co-doped oxyfluoride glasses and glass–ceramics. *J. Lumin.* **2017**, *181*, 25–30. [CrossRef]
38. Moos, H.W. Spectroscopic relaxation processes of rare earth ions in crystals. *J. Lumin.* **1970**, *1*, 106–121. [CrossRef]

39. Binnemans, K. Interpretation of europium(iii) spectra. *Coord. Chem. Rev.* **2015**, *295*, 1–45. [CrossRef]
40. Zollfrank, C.; Scheel, H.; Brungs, S.; Greil, P. Europium(III) orthophosphates: Synthesis, characterization, and optical properties. *Cryst. Growth Des.* **2008**, *8*, 766–770. [CrossRef]
41. Pu, Y.; Tang, K.; Zhu, C.D. Synthesis and luminescence properties of (Y, Gd)(P, V)O4:Eu^{3+}, Bi^{3+} red nano-phosphors with enhanced photoluminescence by Bi^{3+}, Gd^{3+} doping. *Nano-Micro Lett.* **2013**, *5*, 117–123. [CrossRef]
42. Dybowska-Sarapuk, L.; Kielbasinski, K.; Arazna, A.; Futera, K.; Skalski, A.; Janczak, D.; Sloma, M.; Jakubowska, M. Efficient inkjet printing of graphene-based elements: Influence of dispersing agent on ink viscosity. *Nanomaterials* **2018**, *8*, 602. [CrossRef]
43. Huang, L.; Huang, Y.; Liang, J.; Wan, X.; Chen, Y. Graphene-based conducting inks for direct inkjet printing of flexible conductive patterns and their applications in electric circuits and chemical sensors. *Nano Res.* **2011**, *4*, 675–684. [CrossRef]
44. Cui, Z.; Han, Y.; Huang, Q.; Dong, J.; Zhu, Y. Electrohydrodynamic printing of silver nanowires for flexible and stretchable electronics. *Nanoscale* **2018**, *10*, 6806–6811. [CrossRef] [PubMed]
45. Samuel, H.K.; Heuiseok, K.; Kyungtae, K.; Sang, H.L.; Kwan, H.C.; Jun, Y.H. Effect of meniscus damping ratio on drop-on-demand electrohydrodynamic jetting. *Appl. Sci.* **2018**, *8*, 164–172.